

Reconstruction of the Primordial Power Spectrum from CMB

A Thesis

submitted to

Indian Institute of Science Education and Research Pune
in partial fulfillment of the requirements for the
BS-MS Dual Degree Programme

by

Karthik Prabhu P



Indian Institute of Science Education and Research Pune
Dr. Homi Bhabha Road,
Pashan, Pune 411008, INDIA.

April, 2018

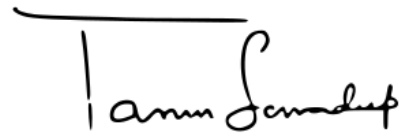
Supervisor: **Dr. Tarun Souradeep**

© **Karthik Prabhu P** 2018

All rights reserved

Certificate

This is to certify that this dissertation entitled **Reconstruction of the Primordial Power Spectrum from CMB**, towards the partial fulfilment of the BS-MS dual degree programme at the Indian Institute of Science Education and Research, Pune represents study/work carried out by **Karthik Prabhu P** at the Inter-University Center for Astronomy and Astrophysics (IUCAA), Pune under the supervision of **Dr. Tarun Souradeep** Inter-University Center for Astronomy and Astrophysics (IUCAA), Pune during the academic year 2017-2018.



Dr. Tarun Souradeep

Committee:

Dr. Tarun Souradeep

Dr. Prasad Subramanian

I gratefully dedicate this thesis to my parents and my sisters
for their endless love and support

Declaration

I hereby declare that the matter embodied in the report entitled **Reconstruction of the Primordial Power Spectrum from CMB** are the results of the work carried out by me at Inter-University Center for Astronomy and Astrophysics (IUCAA), Pune, under the supervision of **Dr. Tarun Souradeep** and the same has not been submitted elsewhere for any other degree.

A handwritten signature in black ink that reads "Karthik". The signature is written in a cursive style with a long horizontal stroke at the end.

Karthik Prabhu P

Acknowledgments

I am highly indebted to Prof. Tarun Souradeep for his constant support and encouragement, right from helping me to decide on a suitable project topic, to introducing me to all the right people in the field. Through the group meetings and the online forum, he helped me gain exposure to new frontiers in CMB research. I also thank Dr. Prasad Subramanian for guiding me as my TAC member. The door to Dr. Subramanian's office was always open whenever I ran into a trouble spot or had a question about my research or writing.

I am thankful to Dr Jayanti Prasad for frequent discussions and ideas that were crucial to my understanding of several concepts. He helped me with the derivations, and also patiently answered several questions I had, particularly with using CosmoMC and the likelihood codes. I am grateful to Dr Dhiraj Hazra, and Dr Arman Shafieloo whose previous work along with Prof. Souradeep formed the foundation of my project. Dhiraj refused to spoon feed me the answers to my doubts and insisted that I struggle with it for a few days, an exercise that greatly benefited me as I would have missed out a few intricate details otherwise. I would also like to thank the graduate students Shabbir, Debabrata, Debajyoti and Rajorshi for discussions on a variety of subjects. I would like to thank both IUCAA and IISER-P for enabling me to carry out this project by providing the necessary computational and bibliographical resources.

Finally, I must express my very profound gratitude to my parents for providing me with unfailing support and continuous encouragement throughout my years of study and through the process of researching and writing this thesis. My friends at IISER provided me with the daily dose of entertaining conversations over lunch and shots of caffeine after that. This accomplishment would not have been possible without them. **Thank you.**

Abstract

The Planck space mission, along with confirming the several predictions of the standard model of Cosmology, has also constrained the six parameters of the Flat Λ CDM model better than ever before. Two of these six parameters model the primordial density fluctuations of the inflaton field while the rest four fix the background cosmology. Several inflationary theories suggest a nearly scale-invariant power-law form for the primordial power spectrum(PPS). However, equipped with the rich data from recent CMB missions, in particular, Planck, it has become possible to reconstruct the PPS in a model-independent non-parametric manner allowing us to relax the theoretically motivated assumptions on the form of PPS. This project can broadly be divided into two parts. In the first part, we demonstrate the efficacy of the Richardson Lucy method in reconstructing the Primordial power spectrum directly from the Planck 2015 temperature data. Assuming the best-fit values for the remaining four background parameters viz. baryonic matter density($\Omega_b h^2$), cold dark matter density($\Omega_c h^2$), optical depth(τ) and acoustic scale parameter(θ), we are able to recover the form of PPS by applying Improved Richardson Lucy Deconvolution method. Our results show features that are absent in the scale-invariant power-law form and were consistent with results from WMAP data. We analyze the reliability of these features and the artifacts of the iRLD method by using smoothing methods. In the latter part of this project, we relax the best-fit values for the background parameters. We explore the 4-dimensional parameter space using a Monte-Carlo sampler called CosmoMC while simultaneously doing the iRLD reconstruction at each point. We obtain new distributions for the background parameters and compared them with the distributions given by Planck collaboration where the Power law model was assumed for the PPS. The results of our analysis indicate changes to the best-fit values of some of the important parameters such as a higher preferred value for the value of Baryon density and the acoustic scale parameter, while the other two parameters, the cold dark matter density and optical depth at reionization tend to prefer a value lower than expected. Our method removes any bias introduced by the assumptions of the model for PPS and thereby allowing us to take an important step in testing predictions of several cosmological models against observations without extraneous theoretical bias. Further extension to this approach that incorporates weak lensing effects and the CMB polarization spectra will lead to final conclusive results.

Contents

Abstract	xi
1 Introduction	1
1.1 Hot Big Bang Cosmology	2
1.2 Friedmann equation	3
1.3 Fluid equation	4
1.4 Acceleration equation	5
1.5 Solving the Friedmann equation	6
1.6 Cosmic Microwave Background	8
1.7 A perfect black-body	10
2 Preliminaries	13
2.1 Statistics of CMB	13
2.2 Cosmic Variance	15
3 Theory	17
3.1 Obtaining the integral equation for C_l	17
3.2 Boltzmann equations	19

3.3 Inflation models and primordial spectrum	22
4 Method of reconstruction	25
4.1 Introduction	25
4.2 RLD method: An application of the Bayes theorem	25
4.3 Integral equation in action	28
4.4 Toy models	29
4.5 Regularization term	29
4.6 Prior bias	31
4.7 Post processing	32
4.8 Convergence criteria	33
4.9 Results	34
5 Cosmological parameter estimation	37
5.1 Markov Chain Monte-Carlo techniques	37
5.2 Metropolis-Hasting algorithm	38
5.3 Likelihood surfaces	39
6 Discussions and Conclusions	41

Chapter 1

Introduction

The field of Astrophysics has witnessed a truly metamorphic transformation in the last fifty years. Bolstered by the rapid progress in science and technology, this field has escaped the realm of of armchair philosophy and has become a rigorous and meticulous science. Although we live in the age of Large Hadron Colliders, they are still a long, long way to go in terms of reaching energies as high as those in the early universe. Hence our cosmos provides us with a vast laboratory to make observations that will not just confirm the existing theories but also reveal new physics that was untouched so far. The discovery of CMB[24] brought along with it a plethora of information about the history and evolution and eventual fate of the universe. However, it is a challenge to develop appropriate statistical tools and techniques to capture all this information from a CMB map portraying the temperature and polarization anisotropies in the sky. Tremendous technological advancements have led to highly accurate measurements of these anisotropies by satellites such as COBE, WMAP and PLANCK[2 1]. This has liberated us from the need to rely on a priori assumptions and models and base our knowledge on concrete observational evidence.

In this thesis we use data from the full sky CMB anisotropy maps provided by the Planck spacecraft to successfully reconstruct the spectrum of density perturbations in the early universe in model-independent, parameter-free manner. This approach has been explored by several groups before, with techniques such as Tikhonov regularisation(Hunt

et al. 2013)[8] , Maximum Entropy deconvolution (Goswami et al. 2013)[25]. We employ the technique of Richardson-Lucy Deconvolution[3] to reconstruct the Primordial Power Spectrum from the Planck 2015 temperature data. We assume the standard model of cosmology with a cosmological constant and the spatial geometry to be Euclidean. We study the features that were missing in our assumptions before and relieve any sort of bias those assumptions had in our estimates of the cosmological parameters to draw intriguing conclusions about the theories that operated the inflationary mechanism.

1.1 Hot Big Bang Cosmology

The success of the Big Bang hypothesis is attributed mainly to the observational confirmation of its predictions of light element abundances, Hubble expansion and the Cosmic Microwave Background radiation. We have information from a myriad of *astronomical messengers* that our universe is expanding with time. It is often represented by a scale factor a , which is set to have a value of unity at the present epoch($a_0 = 1$). The evolution of the scale factor with time depends on the composition or the energy density of the universe. We define another quantity called the Hubble parameter H to quantify the evolution of scale factor. It is defined as,

$$H(t) = \frac{da/dt}{a}. \quad (1.1)$$

At this juncture it is relevant to introduce the Hubble's law describing the expanding universe that quantifies how the physical distance between astronomical bodies changes with time depending on the distance between them.

1.1.1 Hubble's law of the expanding universe

One of the crucial discoveries in Cosmology was the observation that all distant galaxies in our universe around us are moving away from us. Galaxies have characteristic spectral lines that are well known. The observation of redshift in these lines is an indication that the body is moving with some velocity. Edwin Hubble classified the galaxies into groups

and studied their velocities. He found that the galaxies that were farther away from us had higher recessional velocities than the ones closer to us. This came to be known as the **Hubble's law** and the constant of proportionality is called the **Hubble's constant**.

$$\vec{v} = H_0 \vec{r}. \quad (1.2)$$

where \vec{r} is their separation and \vec{v} is their relative velocity.

1.2 Friedmann equation

Einstein laid the foundations for our current understanding of **Standard Model of cosmology** through his general theory of relativity. With the introduction of concepts from mathematics like metrics and geodesics, and relating it to physical concepts like energy density, it became possible to formalize the primitive theories about the creation, evolution and fate of universe into more rigorous terms and cosmology took the shape it has today. The most convenient metric to describe our universe was the 4-dimensional metric with a 3-dimensional maximally symmetric subspace called the Friedmann-Robertson-Walker metric, defined as:

$$ds^2 = dt^2 - a(t)^2 \left[\frac{dr^2}{1 - kr^2} + r^2(d\theta^2 + \sin^2 \theta d\phi^2) \right]. \quad (1.3)$$

Here, k is called the curvature constant. It describes the spatial geometry of the universe we live in. It can take values $-1, 0, +1$ corresponding to hyperbolic, Euclidean and spherical(closed) universes respectively. The Einstein's field equation allows us to relate the geometry of our universe to its energy content through this equation:

$$R_{\mu\nu} - \left(\frac{1}{2}R - \Lambda \right) g_{\mu\nu} = \frac{8\pi G}{c^4} T_{\mu\nu}. \quad (1.4)$$

where, $R_{\mu\nu}/R$, the Ricci tensor/scalar and the metric tensor g describe the structure of space-time, T , the stress energy tensor describes the energy and momentum density, G and c are the usual fundamental constants of gravitation and the universal speed of light, and Λ represents the cosmological constant. By assuming the universe to be composed of

a perfect fluid with isotropic pressure p and energy density ρ with $u^{(i)}$ being the velocity vector, we can write the energy-momentum tensor as

$$T_{\mu\nu}^{(i)} = -p_i g_{\mu\nu} + (p_i + \rho_i) u_{\mu}^{(i)} u_{\nu}^{(i)}. \quad (1.5)$$

This leads to the Friedmann equation:

$$\left(\frac{\dot{a}}{a}\right)^2 = \frac{8\pi\rho G}{3} - \frac{kc^2}{a^2}. \quad (1.6)$$

This describes the evolution of the scale factor in terms of the energy density and spatial curvature of the universe.

1.3 Fluid equation

The fluid equation describes how the density of the fluid in the universe evolves with time depending on the kind of the fluid. From the first law of thermodynamics we have,

$$dE + pdV = TdS. \quad (1.7)$$

This equation is applied to a fluid of expanding volume V . We assume the co-moving distance to be unity. So the physical radius will be just a . Using $E = mc^2$,

$$E = \frac{4\pi}{3} a^3 \rho c^2. \quad (1.8)$$

Differentiating with respect to time,

$$\frac{dE}{dt} = 4\pi\rho c^2 a^2 \frac{da}{dt} + \frac{4\pi}{3} a^3 \frac{d\rho}{dt} c^2. \quad (1.9)$$

Differentiating volume with respect to time,

$$\frac{dV}{dt} = 4\pi a^2 \frac{da}{dt}. \quad (1.10)$$

We assume the expansion to be reversible. Therefore, $dS = 0$ or $dE = -pdV$

$$4\pi\rho c^2 a^2 \dot{a} + \frac{4\pi}{3} a^3 \dot{\rho} c^2 = -p 4\pi a^2 \dot{a}. \quad (1.11)$$

By appropriate cancellation and rearrangement we get,

$$\dot{\rho} + 3\frac{\dot{a}}{a} \left(\rho + \frac{p}{c^2} \right) = 0. \quad (1.12)$$

This is akin to the first law of thermodynamics eqn.(1.7) in the special case of isentropic processes. Equation (1.12) is called the fluid equation. The density changes due to two sources. The decrease in the density due to the increase in the volume, and the other arises from energy loss owing to the work done as the Universe's volume increased.

1.4 Acceleration equation

We can use the previous two equations to derive a new equation that describes the acceleration of the scale factor.

Differentiating eqn.(1.6) with respect to time we obtain,

$$2\frac{\dot{a}}{a} \frac{a\ddot{a} - \dot{a}^2}{a^2} = \frac{8\pi G}{3} \dot{\rho} + 2\frac{kc^2 \dot{a}}{a^3}. \quad (1.13)$$

and substituting for $\dot{\rho}$ from 1.12 we obtain,

$$\frac{\ddot{a}}{a} - \left(\frac{\dot{a}}{a} \right)^2 = -4\pi G \left(\rho + \frac{p}{c^2} \right) + \frac{kc^2}{a^2}. \quad (1.14)$$

Substituting equation 1.6 again, we get,

$$\frac{\ddot{a}}{a} = -\frac{4\pi G}{3}\left(\rho + \frac{3p}{c^2}\right). \quad (1.15)$$

Note that the constant k cancels out and doesn't appear in the acceleration equation. If the fluid has any pressure it increases the gravitational force and further decelerates the expansion of the universe.

1.5 Solving the Friedmann equation

The solutions of the Friedmann equation gives us an idea about how the universe will evolve with time. However, as we have seen before, this equation contains a density term in it. We need to know what the universe is made up of. Consider two cases in a model of the universe with vanishing spatial curvature ($k = 0$); one in which the universe is made up of matter (non-relativistic only), another universe that is made of radiation.

1.5.1 Matter

In cosmology, matter is understood to be non-relativistic matter only. From the equation of state we have pressure $p=0$ for matter.

$$\dot{\rho} + 3\frac{\dot{a}}{a}\rho = 0. \quad (1.16)$$

$$\implies \frac{1}{a^3} \frac{d}{dt}(\rho a^3) = 0. \quad \implies \frac{d}{dt}(\rho a^3) = 0 \quad (1.17)$$

$$\implies \rho \propto a^{-3}. \quad (1.18)$$

This is not very surprising. Density falls as the cube of volume. The advantage of

choosing $k=0$ in our equations is that we can rescale $a(t)$ as we want since \dot{a}/a occurs in the equation. We can very conveniently choose $a = 1$ at the current time. If $\rho = \rho_0$ at current time, we have,

$$\rho = \frac{\rho_0}{a^3}. \quad (1.19)$$

Substituting for ρ with $k=0$ in the Friedmann equation we get

$$\dot{a}^2 = \frac{8\pi G\rho_0}{3} \frac{1}{a}. \quad (1.20)$$

Solving this separable equation, we get,

$$a(t) \propto t^{2/3}. \quad (1.21)$$

Taking $a = 1$ at current time $t = t_0$

$$a(t) = \left(\frac{t}{t_0}\right)^{2/3}. \quad ; \quad \rho(t) = \frac{\rho_0}{a^3} = \frac{\rho_0 t_0^2}{t^2}. \quad ; \quad H \equiv \frac{\dot{a}}{a} = \frac{2}{3t}. \quad (1.22)$$

Such an universe expands forever. However, as time progresses the rate of expansion becomes slower.

1.5.2 Radiation

The equation of state tells us that $p = \rho c^2/3$ for radiation.

$$\dot{\rho} + 4\frac{\dot{a}}{a}\rho = 0. \quad (1.23)$$

Following the same steps as the previous case, we get,

$$\rho \propto a^{-4}. \quad (1.24)$$

$$a(t) = \left(\frac{t}{t_0}\right)^{1/2} \quad ; \quad \rho(t) = \frac{\rho_0}{a^4} = \frac{\rho_0 t_0^2}{t^2} \quad ; \quad H \equiv \frac{\dot{a}}{a} = \frac{1}{2t}. \quad (1.25)$$

Such an universe expands slower than one dominated by matter. The extra power that further causes the drop in density is due to the stretching of wavelength of light.

Having found out the evolution of rate of expansion for two kinds of universes, we have to apply it to our universe which is composed of a mixture of matter and radiation. By assuming one of the component to be dominant we solve the equations and obtain solutions.

For the radiation dominated universe:

$$a(t) \propto t^{1/2} \quad ; \quad \rho_{rad} \propto \frac{1}{t^2} \quad ; \quad \rho_{mat} \propto \frac{1}{a^3} \propto \frac{1}{t^{3/2}}. \quad (1.26)$$

The density in matter falls off slower than the density in radiation. Eventually the radiation domination will end and matter will begin to dominate.

$$a(t) \propto t^{2/3} \quad ; \quad \rho_{mat} \propto \frac{1}{t^2} \quad ; \quad \rho_{rad} \propto \frac{1}{a^4} \propto \frac{1}{t^{8/3}}. \quad (1.27)$$

In this case the matter will continue to dominate over radiation. Therefore, whatever be the case, after long enough time, matter will dominate. The transition between radiation to matter domination will be characterized by an increase in the expansion rate from $a(t) \propto t^{1/2}$ to the $a(t) \propto t^{2/3}$ law.

1.6 Cosmic Microwave Background

According to the Big Bang theory, the early universe was a hot and dense plasma of protons, electrons and photons. Any atom formed would be instantly annihilated by a high energy photon. Due to a large number of events of scattering of photons by the free electrons, the mean free path of photons was so short that the medium was practically opaque

to electromagnetic radiations. Matter and radiation were at a thermal equilibrium due to these scattering events. Gradually as the universe expanded and cooled down, the conditions became feasible for the formation of the hydrogen atom. Electrons were bound to the nucleon core and neutral atoms were formed. This event is called **Recombination**. The photons decoupled from these electrons and started moving freely without interacting with baryons, an event known as **photon decoupling**. We see these photons today as the *Cosmic Microwave Background*. The surface where the photons and electron decoupled is called the surface of last scattering. Whatever imperfections existed from a homogeneous universe on this surface, leaves their signatures on the photons that were decoupled at that time. They manifest as anisotropies and inhomogeneities in the CMB that we observe today and hence it is a window into the past.

The Cosmic Microwave Background is the relic radiation of the Big Bang that happened about 13.8 billion years ago. It was initially predicted by George Gamov and Ralph Alpher in 1948. They speculated that there has to be a uniform background temperature around 5K. In 1965, Penzias and Wilson^[24] published their findings of the unaccounted excess of the temperature measured by their radiometer that was immediately identified as the CMB radiation. Given the huge cosmological significance of the CMB signal, it launched a great push to analyze this microwave background and this ushered in an era of observational cosmology.

COsmic Background Explorer (COBE) was the first space mission that measured the map of the intensity(temperature) of the CMB on the full sky. COBE was a successful mission that confirmed two important predictions of the Big Bang theory: that the CMB has a almost perfect black-body spectrum, and that it has small inhomogeneities. George Smoot and John Mather, who led this mission, won the Nobel prize in Physics in 2006. The advent of satellites like WMAP and Planck further advanced our understanding of our universe by providing increasingly accurate measurements of CMB temperature and linear polarization. Today there are also several ground based experiments like BICEP and KECK that are using cutting edge technology to make increasingly accurate measurements of CMB.

1.7 A perfect black-body

As discussed earlier the matter and radiation were in thermal equilibrium before the event of decoupling thanks to the scattering processes. According to Planck's law, a black-body spectrum is a characteristic of its temperature and the energy density of photons between frequencies ν and $\nu + d\nu$ at a temperature T is given by,

$$\epsilon(\nu)d\nu = \frac{8\pi h}{c^3} \frac{\nu^3 d\nu}{\exp(h\nu/k_B T) - 1}. \quad (1.28)$$

where k_B is the Boltzmann constant h is the Planck's constant and c is the speed of light in vacuum. The total energy density of the spectrum can be found by integrating the above equation over all frequencies. Set $x = h\nu/k_B T$,

$$\epsilon = \frac{8\pi k_B^4}{h^3 c^3} T^4 \times \int_0^\infty \frac{x^3 dx}{e^x - 1}. \quad (1.29)$$

The integral gives $\pi^4/15$

$$\epsilon = \alpha T^4. \quad (1.30)$$

where $\alpha = 7.56 \times 10^{-16} \text{Jm}^{-3}\text{K}^{-4}$. This is the Stefan-Boltzmann constant.

We have seen earlier that for radiation, the following relation holds between temperature T and scale factor a

$$T \propto \frac{1}{a}. \quad (1.31)$$

After the decoupling, the blackbody energy distribution was retained in isentropic expansion. This can be easily seen through an heuristic argument about a special property of the equation for energy density. Let us assume that the photons went from being in thermal equilibrium with matter to free streaming. As the universe expands, the frequency of a photon falls as $1/a$, just like the temperature. Since the quantity in the denominator is a function of ν/T it stays invariant. The quantity in the numerator however scales as the inverse cube of the scale factor. But this is taken care by the increased volume which is proportional to the cube of the scale factor. Therefore as the universe expands it preserves its spectrum, however at a temperature scaled down by the expansion factor of the universe.

We can estimate when the CMB formed, i.e., the time of decoupling by some simple calculations. From thermodynamics, we know that the mean energy of a photon in a black-body distribution is $3k_B T$. The ionization energy of hydrogen atom is about 13.6eV. Therefore, the temperature at decoupling is,

$$T \approx \frac{13.6}{3k_B} = 50,000\text{K}. \quad (1.32)$$

But this estimate is very crude since there are far more photons in our universe than electrons, about a factor of 10^9 . Hence, even if the mean energy was less than 13.6eV, we would still have enough photons towards the tail of the spectrum to ionize the hydrogen atoms and a chemical balance equation, better known as the Saha ionization formula needs to be used. Taking this into consideration and by integrating over the photon distribution, it has been concluded that the temperature at the time of decoupling was around 3000K.

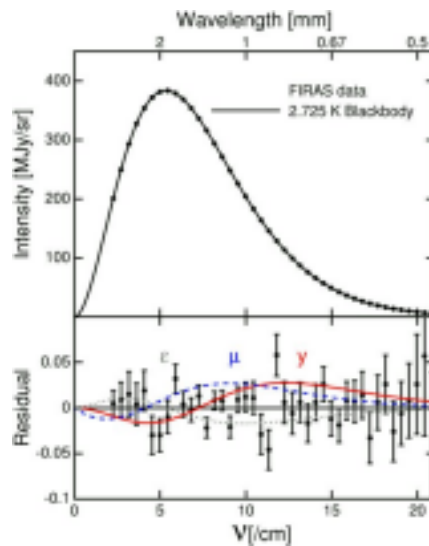


Figure 1.1: This figure represents the intensity of the CMB radiation as a function of frequency from the data obtained by FIRAS instrument on the COBE satellite. The error bars are too small to be even visible. The CMB radiation is the nature's most perfect realization of a black-body radiation.

Chapter 2

Preliminaries

2.1 Statistics of CMB

2.1.1 The cosmological principle

The cosmological principle is of fundamental importance in modern cosmology. It tells us that the universe looks same to you no matter where you are in it, when statistically averaged on a sufficiently large scale. We believe that at large scales above a few hundred mega parsecs, our universe is homogeneous and isotropic which means that it is the same at all points and same in all directions respectively. The photons that started their journey of free streaming post-recombination were subjected to several physical phenomena that left imprints on their distribution. This information can be captured in the form of anisotropies in the CMB temperature and a pattern of linear polarization.

2.1.2 Spherical harmonic basis

We express the temperature anisotropies as $\Delta T(\hat{n}) = T(\hat{n}) - T_0$, where T_0 is the average temperature of the CMB = 2.725K, a distribution which has an expectation value equal to

zero and some non-zero variance. $\hat{n} = (\theta, \phi)$ is a general direction in the sky. Cosmologists frequently employ the spherical harmonics basis to represent these anisotropies as a function of multipole l since it is a 2d field measured on the sky.

$$\frac{\Delta T}{T}(\hat{n}) = \sum_l a_{lm} Y_{lm}(\theta, \phi). \quad (2.1)$$

A predicate of the Cosmological principle is that CMB anisotropy is expected to be statistically isotropic and Gaussian. Therefore the two point correlation function must contain all the information encoded in the field.

$$C_{ij} \equiv C(\hat{n}_i, \hat{n}_j) = \langle \Delta T(\hat{n}_i) \Delta T(\hat{n}_j) \rangle. \quad (2.2)$$

Since CMB is statistically isotropic, we have

$$C(\hat{n}_i, \hat{n}_j) = C(\mu), \quad \mu = \arccos(\hat{n}_i \cdot \hat{n}_j). \quad (2.3)$$

Since the two-point function is a function of just the angular separation θ it would be convenient to express it in terms of Legendre polynomials.

$$C(\theta) = \frac{1}{4\pi} \sum_{l=2}^{\infty} (2l+1) C_l P_l(\cos \theta). \quad (2.4)$$

The quantity C_l^{AB} , where A,B=T-Temperature, E-Gradient mode of polarization, B-Curl mode of polarization, is known as *angular power spectrum*. Since this is a complete basis, it describes the whole of CMB anisotropy under the aforementioned assumptions. The monopole term $l = 0$ corresponds to the mean temperature of CMB. There is a contribution to the temperature of the order of mK which is due to the local motion of the observer through the universe corresponding to $l = 1$. Both these terms are not of cosmological significance and are subtracted while studying CMB anisotropies. Since we are dealing with only temperature maps in this project, we shall henceforth drop the superscript indicating temperature. We define another quantity related to the angular power spectrum $D_l = l(l+1)C_l/2\pi$ that corresponds to the power per log interval of the multipole and plot it against l as shown in the figure [2.1](#)

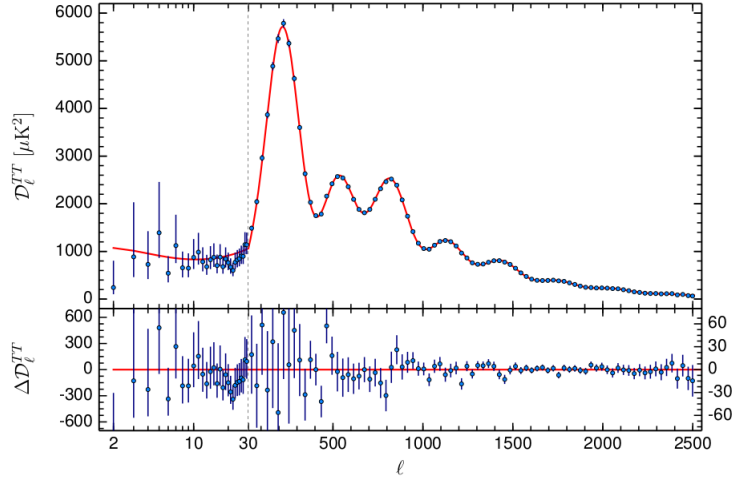


Figure 2.1: Temperature power spectrum from the Planck 2015 data. The theoretical curve from the best-fit Λ CDM cosmology is plotted against the Planck TT + low P data. (Figure is from [1])

The predicted angular power spectra that I have used in this project are numerically computed by a publicly available program called CAMB(Code for Anisotropies in the Microwave Background) which generates a set of C_l 's for a given set of cosmological parameters.

2.2 Cosmic Variance

From equation (2.4) we have

$$\langle a_{lm} a_{l'm'}^* \rangle = C_l \delta_{ll'} \delta_{mm'}.$$

However, the ensemble average can not be performed in practice, from our single vantage point of observation. The best we can do is write an estimator for C_l as follows:

$$C_l^{\text{est}} = \frac{1}{2l+1} \sum_{m=-l}^l |a_{lm}|^2. \quad (2.5)$$

with an inherent unsurmountable bound on how well can we recover the angular power spectrum at different angular scales from our observations.

$$\sigma_{C.V.} \equiv \langle (C_l - C_l^{est})(C_{l'} - C_{l'}^{est}) \rangle = \frac{2}{2l+1} C_l^2 \delta_{ll'}. \quad (2.6)$$

There is an inherent lack of information for large angular separations due to smaller sample size. If there is instrument noise also present, the revised variance in C_l becomes,

$$\sigma_{C.V.+noise} \equiv \langle (C_l - C_l^{est})(C_{l'} - C_{l'}^{est}) \rangle = \frac{2}{2l+1} [C_l^s + C_l^N B_l^{-2}]^2 \delta_{ll'}. \quad (2.7)$$

where B_l is the beam function that describes how the detector beam response function is spread out around the pointing direction.

Chapter 3

Theory

3.1 Obtaining the integral equation for C_l

Angular surveys are the most fundamental probes of inhomogeneities and anisotropies in cosmology. The basic measure used is the two point correlation function. In real space it is the angular correlation function and in Fourier space it becomes the 2-dimensional power spectrum. The measurements of the temperature anisotropies are converted to more tractable angular correlation function in the following manner. Let the anisotropy in temperature at a location ($x = 0$) be denoted by

$$\Delta(\mathbf{x} = \mathbf{0}, \hat{n}, \tau_0) = \Delta T/T_0 = \sum_{lm} a_{lm} Y_{lm}. \quad (3.1)$$

In terms of Fourier space,

$$\Delta(\mathbf{x}, \hat{n}, \tau) = \int \frac{d^3k}{(2\pi)^3} e^{i\mathbf{k}\cdot\mathbf{x}} \Delta(\mathbf{k}, \hat{n}, \tau). \quad (3.2)$$

The dependence on \hat{n} comes only in the form of $\mathbf{k}\cdot\hat{n}$ [9]. Separating the radiative transfer function and gravitational potential terms,

$$\Delta(\mathbf{k}, \hat{n}, \tau) = \Phi(\mathbf{k}, \tau) \tilde{\Delta}(k, \hat{k} \cdot \hat{n}, \tau).$$

Expanding the second term on RHS using Legendre polynomials, we get,

$$\Delta(\mathbf{x}, \hat{n}, \tau) = \int \frac{d^3k}{(2\pi)^3} e^{i\mathbf{k}\cdot\mathbf{x}} \Phi(\vec{k}) \sum_{l=0}^{\infty} (-i)^l (2l+1) \Delta_l(k, \tau_0) P_l(\mathbf{k} \cdot \hat{n}). \quad (3.3)$$

Using the relation between Legendre polynomials and Spherical harmonics, we can write (7) as,

$$\Delta(\mathbf{x}, \hat{n}, \tau) = \int \frac{d^3k}{(2\pi)^3} e^{i\mathbf{k}\cdot\mathbf{x}} \Phi(\vec{k}) 4\pi \sum_{lm} (-i)^l \tilde{\Delta}(k, \tau) Y_{lm}^*(\hat{k}) Y_{lm}(\hat{n}). \quad (3.4)$$

Therefore, from eq. 2.5 and 2.8, we have

$$a_{lm} = (-i)^l 4\pi \int \frac{d^3k}{(2\pi)^3} \Phi(\mathbf{k}) \tilde{\Delta}(k, \tau_0) Y_{lm}^*(\hat{k}). \quad (3.5)$$

We define the power spectrum of the potential fluctuations as

$$\langle \Phi(\mathbf{k}) \Phi(\mathbf{k}') \rangle = (2\pi)^3 P_{\Phi}(k) \delta(\mathbf{k} - \mathbf{k}'). \quad (3.6)$$

We obtain the two point correlation function as,

$$C_l = \langle a_{lm} a_{l'm'}^* \rangle = e^{-i\frac{\pi}{2}(l-l')} (4\pi)^2 \int \frac{d^3k}{(2\pi)^3} \int \frac{d^3k'}{(2\pi)^3} \langle \Phi(\mathbf{k}) \Phi^*(\mathbf{k}') \rangle \Delta_l(k, \tau_0) \Delta_{l'}^*(k', \tau_0) Y_{lm}^*(\hat{k}) Y_{l'm'}(\hat{k}')$$

. Substituting from eq. 2.10

$$\begin{aligned} &= e^{-i\frac{\pi}{2}(l-l')} (4\pi)^2 \int \frac{d^3k}{(2\pi)^3} P_{\Phi}(k) \Delta_l(k, \tau_0) \Delta_{l'}^*(k, \tau_0) Y_{lm}^*(\hat{k}) Y_{l'm'}(\hat{k}) \\ &= e^{-i\frac{\pi}{2}(l-l')} (4\pi)^2 \int \frac{dk}{(2\pi)^3} k^2 P_{\Phi}(k) \Delta_l(k, \tau_0) \Delta_{l'}^*(k, \tau_0) \int d\Omega Y_{lm}^*(\hat{k}) Y_{l'm'}(\hat{k}) \end{aligned}$$

Using the fact that $\int d\Omega Y_{lm}^*(\hat{k}) Y_{l'm'}(\hat{k}) = \delta_{ll'} \delta_{mm'}$

$$= 4\pi \int \frac{dk}{k} \frac{k^3 P_{\Phi}(k)}{2\pi^2} |\Delta_l(k, \tau_0)|^2$$

We define a dimensionless quantity, $\mathcal{P}(k) = k^3 P_{\Phi}(k) / 2\pi^2$, corresponding to power per

log interval of wavenumber.

$$C_l = 4\pi \int \frac{dk}{k} \mathcal{P}(k) |\Delta_l(k, \tau_0)|^2. \quad (3.7)$$

Henceforth, for the simplicity of notation and making it suitable for numerical integration, we shall use this equation. [\[4\]](#) [\[5\]](#)

$$C_l = \sum_k G_{lk} P_k. \quad (3.8)$$

where, $G_{lk} = 4\pi \frac{dk}{k} |\Delta_l(k, \tau_0)|^2$. In the equation above, the term G_{lk} is fixed by the background parameters of the assumed cosmology. It also contains information about the projection from a 3D wavenumber space to the multipole space. The other term P_k contains information about the primordial density fluctuations. However, the observable quantity we will be dealing with is the two point correlation function, C_l which the Planck satellite has measured to a high accuracy upto $l = 2500$. The functional form of primordial part P_k is dictated by the underlying theory which is at best an educated guess. However, equipped with the rich data made available by satellites like Planck and WMAP, given the matrix G_{lk} , it is a matter of deconvolution to reconstruct the form of PPS.

3.2 Boltzmann equations

The radiative transfer kernel encodes how the anisotropies evolve over time. Our aim is to get $\tilde{\Delta}_l(k, \tau_0)$ from $\tilde{\Delta}_l(k, \tau < \tau_{rec})$. The solution to the Boltzmann equation describe how it happens. We simplify things by assuming only two distinct regimes with a reasonably sharp boundary. One, before the recombination where there are strong collisions, and second when there is free streaming of photons, or the collisions are negligible. The Boltzmann equation looks like this.

$$\frac{df}{dt} = c[f]. \quad (3.9)$$

where, $c[f]$ is the collision term and f denotes the phase space distribution function for photons. We expand f to a linear order as $f = f^0 + \delta f$. As discussed above, we consider

two regimes,

$$\tau < \tau_{rec}; \quad c[f] \text{ is strong}$$

$$\tau > \tau_{rec}; \quad c[f] = 0$$

.

We are now in a position to evolve the radiative kernel part of the angular power spectrum from the time of recombination to today. Using fluid approximation, we have need to consider Δ_0 and Δ_1 terms in the Taylor expansion. Δ_0 is called the monopole term which describes the density fluctuations and Δ_1 is the dipole term which describes the velocity of baryons.

3.2.1 Free streaming region

Consider $\tilde{\Delta}_l(k, \tau_s)$ going to $\tilde{\Delta}_l(k, \tau_0)$, where τ_s is well inside the free streaming region. Let τ any instance of time in between τ_s and τ_0 .

$$\tilde{\Delta}(\vec{k}, \hat{n}, \tau) = e^{i\hat{n}\cdot\vec{k}(\tau-\tau_s)} \tilde{\Delta}(\vec{k}, \hat{n}, \tau_s). \quad (3.10)$$

In the absence of the collision term, Boltzmann equation is just a plane wave propagation. We can write the overall equation as,

$$\tilde{\Delta}(|\vec{k}|, \hat{k} \cdot \hat{n}, \tau) = \sum_l (-i)^l (2l+1) \tilde{\Delta}(k, \tau) P_l(\hat{k} \cdot \hat{n}). \quad (3.11)$$

$$\tilde{\Delta}_l(k, \tau) = \frac{1}{2(-i)^l} \int_{-1}^{+1} d\mu \tilde{\Delta}(k, \mu, \tau) P_l(\mu). \quad (3.12)$$

Using the Bessel function expansion for exponential function,

$$e^{i\hat{n}\cdot\hat{k}(\tau-\tau_s)} = \sum_L (-i)^l (2L+1) j_L(k\Delta\tau) P_L(\hat{k} \cdot \hat{n}). \quad (3.13)$$

where $\Delta\tau = \tau - \tau_s$. Substituting this in the previous equation we get,

$$\tilde{\Delta}_l(k, \tau) = \frac{1}{2(-i)^l} \int_{-1}^{+1} d\mu \left[\sum_{L'} (-i)^{l'+L} (2l' + 1)(2L + 1) j_L(k\Delta\tau) \tilde{\Delta}_{l'}(k\Delta\tau_s) P_{l'}(\mu) P_L(\mu) \right] P_l(\mu). \quad (3.14)$$

$$= \frac{1}{2} \sum_{L'} (-i)^{l'+L-l} (2l' + 1)(2L + 1) j_L(k\Delta\tau) \tilde{\Delta}_{l'}(k\Delta\tau_s) \int_{-1}^{+1} d\mu P_{l'}(\mu) P_L(\mu) P_l(\mu). \quad (3.15)$$

We use a standard result to replace the integral,

$$\int_{-1}^{+1} d\mu P_{l'}(\mu) P_L(\mu) P_l(\mu) = \frac{2}{2L + 1} \left[C_{l0l'0}^{L0} \right]^2. \quad (3.16)$$

where, \mathcal{C} is called the Clebsch Gordan coefficient.

$$\Delta_l(k\Delta\tau) = \sum_{l'L} (-i)^{l'+L-l} (2l' + 1) j_L(k\Delta\tau) \tilde{\Delta}_{l'}(k\Delta\tau_s) \left[C_{l0l'0}^{L0} \right]^2. \quad (3.17)$$

$$\Delta_l = \sum_{l'} A_{ll'}(\Delta\tau) \tilde{\Delta}_{l'}(k\Delta\tau_s); \quad A_{ll'} = \sum_L (-i)^{l+l'+L} j_L(k\Delta\tau) \left[C_{l0l'0}^{L0} \right]^2. \quad (3.18)$$

Now, we use the approximation where there is only the monopole term present.

$$\tilde{\Delta}_{l'}(k\Delta\tau_s) = \tilde{\Delta}_0(k\Delta\tau_s) \delta_{l'0}. \quad (3.19)$$

$$\implies \tilde{\Delta}_l(k\Delta\tau) = \sum_L (-i)^{l-L} j_L(k\Delta\tau) \tilde{\Delta}_0(k\Delta\tau_s) \left[C_{l000}^{L0} \right]^2. \quad (3.20)$$

Using another standard result [\[11\]](#),

$$C_{lm00}^{LM} = \delta_{lL} \delta_{mM} \implies C_{l000}^{L0} = \delta_{lL}. \quad (3.21)$$

$$\tilde{\Delta}_l(k\Delta\tau) = j_l(k\Delta\tau) \tilde{\Delta}_0(k\Delta\tau_s). \quad (3.22)$$

Going back to the expression for angular power spectrum,

$$\implies C_l = 4\pi \int \frac{dk}{k} \frac{(k^3 P_\phi)}{2\pi^2} j_l^2(k\Delta\tau) |\Delta_0(k\Delta\tau)|^2. \quad (3.23)$$

From Sachs-Wolfe effect, we have $\Delta_0 = 1/3$.

$$C_l = \frac{4\pi}{9} \int \frac{dk}{k} \left(\frac{k^3 P_\phi}{2\pi^2} \right) j_l^2(k\Delta\tau). \quad (3.24)$$

For Harrison-Zeldovich Spectrum $(\frac{k^3 P_\phi}{2\pi^2}) = A$ and the integral evaluates to $4/\pi$. Therefore,

$$C_l = \frac{4\pi}{9} A \int \frac{dk}{k} j_l^2(k\Delta\tau) = \frac{16/9}{l(l+1)} A. \quad (3.25)$$

For a general case,

$$C_l = \frac{4\pi}{9} \int \frac{dk}{k^2} |\delta_k|^2 j_l^2(k\Delta\tau). \quad (3.26)$$

For a power-law, $|\delta_k|^2 = Ak^n$.

$$C_l = \frac{4\pi A}{9} \frac{\Gamma(3-n)\Gamma((2l+n-1)/2)}{\Gamma^2((4-n)/2)\Gamma((2l+5-n)/2)}. \quad (3.27)$$

We have only considered the first term in the expansion. We could add the second term, the dipole, and then solve it in a similar way although it gets slightly more complicated. It is left as an exercise to the math romantics.

3.3 Inflation models and primordial spectrum

3.3.1 Scale invariant power law model

Most of the inflationary models that we have at our disposal, suggest an almost scale invariant power law for the primordial power spectrum. The functional form is usually written as

$$P_k = A_s (k/k_*)^{n_s-1}. \quad (3.28)$$

If $n_s = 1$, it becomes a scale invariant spectrum, also known as Harrison-Zeldovich-Peebles spectrum. For this special case, $P_k = A_s = \text{constant}$. We have, $C_l = \text{constant} \int_0^\infty \frac{dk}{k} \Delta_l(k)^2 = \frac{1}{2(l)(l+1)} \cdot \text{constant}$. This is why we plot $D_l = \frac{l(l+1)}{2\pi} C_l$. For a scale invariant spectrum, we get a flat Sachs-Wolfe part of C_l . The current data are pretty much consistent with a nearly scale invariant spectrum. They suggest a small tilt ($n_s < 1$). We are interested to look for other scale dependent features that can match the observations with tighter constraints. Although most of the inflation models predict a scale invariant power law form for the primordial power spectrum, it is possible to incorporate certain scale dependent features by making small modifications to the power law. The current observations tell us that the form of PPS very closely resembles the power law. However some anomalies in the angular power spectrum such as the low power at lower multipoles motivate us to look towards other inflation models specifically those that tend to have a low l cutoff. will discuss some simple models below.

3.3.2 Exponential cutoff model (EC)

[15] One of the simplest modification that we can do to the power law, by addition of a minimal number of extra parameters is to add an exponentially decaying function to represent the low l cutoff. The functional form looks something like this.

$$P(k) = A_s k^{n_s-1} [1 - e^{-(k/k_*)^\alpha}] \quad (3.29)$$

Here, α is the additional parameter that determines the sharpness of the cutoff.

3.3.3 Starobinsky Model (SB)

[14] Starobinsky has discussed the possibility of broken scale-invariant models for inflation with localised spikes and steps which can create cutoffs in the primordial power spectrum. The modification to the PPS is expressed as a multiplicative factor to the regular PPS as follows.

$$P(k) = P_0(k) \mathcal{D}^2(y, R_*). \quad (3.30)$$

and,

$$\mathcal{D}^2(y, R_*) = [1 - 3(R_* - 1) \frac{1}{y} ((1 - \frac{1}{y^2}) \sin 2y + \frac{2}{y} \cos 2y) + \frac{9}{2}(R_* - 1)^2 \frac{1}{y^2} (1 + \frac{1}{y^2}) \times (1 + \frac{1}{y^2} + (1 - \frac{1}{y^2}) \cos 2y)] \quad (3.31)$$

where, $y = k/k_*$, and R_* is a new parameter that determines the slope of the power spectrum. There are other models such as the Pre-inflationary Kinetic Domination model(KD) and Pre-inflationary Radiation domination model(VF) which we shall not be discussing here. However the figure below demonstrates the form of the PPS these models suggest.

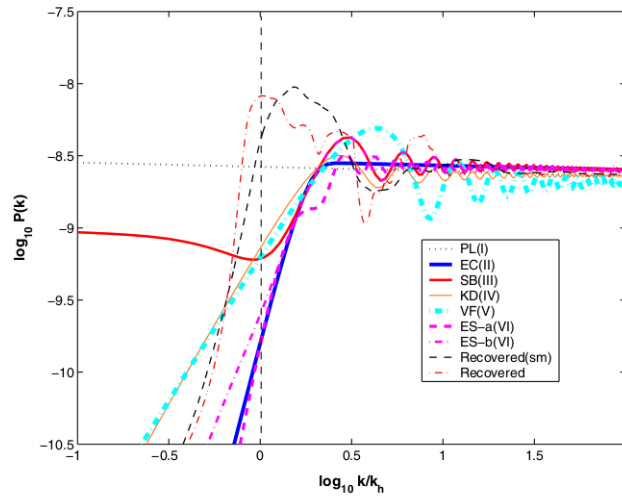


Figure 3.1: This figure represents PPS generated by several different inflation models. There is also the PPS recovered directly from the WMAP data for comparison. (figure is from [13]).

Chapter 4

Method of reconstruction

4.1 Introduction

Based on the discussion in Chapter 2, we conclude that in order to obtain $P(k)$, given C_l and G_{lk} , what we have at hand is essentially a problem of deconvolution. There are several techniques developed particularly in the field of signal processing and image processing that are used to find a solution of a convolved equation. Since we know the transfer function well for any given cosmological model, we can apply one such algorithm that has been extensively used in Astronomy and other areas to recover pure images that have been blurred by some point spread function. This is the Richardson Lucy Deconvolution Algorithm(RLD)[\[3\]](#). It was introduced by William Richardson and Leon Lucy, independently, in 1972.

4.2 RLD method: An application of the Bayes theorem

The Bayesian approach to inference makes use of prior knowledge about conditions related to events to make comments about the probability of a particular event and how on the basis of availability of new data, one should logically update one's assessment about

these probabilities. We use Bayes theorem to update our priors using data to get posterior beliefs using Bayes theorem. The statement of the theorem is as follows:

$$P(\theta|X) = \frac{P(X|\theta)P(\theta)}{\sum_{\theta} P(X|\theta)P(\theta)}. \quad (4.1)$$

where $P(X) \neq 0$

$P(\theta)$ is interpreted as our prior knowledge about the probability of event θ , which in our case is the parameter we are interested in estimating,

$P(X|\theta)$ is called the likelihood, that is the probability of observing data X , given the parameter is θ ,

$P(\theta|X)$ is called the posterior belief, that is how we update our prior based on availability of new information X .

4.2.1 In the language of cosmology...

We are interested in obtaining the primordial power spectrum P_k , from the observed angular power spectrum C_l s. The angular power spectrum is a convolution of primordial power spectrum with an evolution kernel G_{lk} and is given by

$$C_l = \sum_k G_{lk} P_k \quad (4.2)$$

If the kernel G_{lk} were invertible this would be a simple problem of matrix inversion. However, we have a C_l each for l values ranging from 2-2508, 2897 k values between $7.10e-06$ and 0.47 . This is an ill-conditioned system of linear equations. The observed angular power spectrum is a convolution of a cosmological radiative transport kernel with an assumed primordial power spectrum. The fact that P_k , C_l and G_{lk} are strictly positive quantities is just icing on the cake, making RLD algorithm a much-suited method to de-project the primordial power spectrum from the 2D angular power spectrum. We make the best possible guess for our prior $P_k^{(i)}$, and iteratively update it until get $C_l^{(i)}$ s that match closely with the observed $C_l^{(D)}$ [6, 7, 8]. The derivation stems from probability theory and is as follows. To make our case, we construct the following one-dimensional probability

distributions:

$$\sum_k \tilde{P}_k = 1; \quad \sum_l \tilde{C}_l = 1; \quad (4.3)$$

We can view the radiative kernel as a conditional probability distribution.

$$\sum_l \tilde{G}_{lk} = 1; \quad (4.4)$$

Doing this normalization allows us to jump between the language of probability and cosmology without loss of rigor. Let L_{kl} be the last remaining piece required for completing the Bayes theorem. We are now in a position to state the Bayes theorem in the language of cosmology.

$$\tilde{P}_k \tilde{G}_{lk} = \tilde{C}_l L_{kl}. \quad (4.5)$$

Or,

$$L_{kl} = \frac{\tilde{P}_k}{\tilde{C}_l} \tilde{G}_{lk}. \quad (4.6)$$

Integrating equation 3.5 with dl , we have

$$\tilde{P}_k = \int \tilde{C}_l L_{kl} dl. \quad (4.7)$$

For convenience of numerical analysis, we discretize it in the form,

$$\tilde{P}_k = \sum_l \tilde{C}_l L_{kl}. \quad (4.8)$$

We begin with a uniform prior $P_k^{(0)}$. This corresponds to a power spectrum $C_l^{(0)}$. Substituting from equation 3.6 and with the aim of ultimately matching $C_l^{(i)}$ with the data $C_l^{(D)}$, we update our prior as follows,

$$P_k^{(i+1)} = P_k^{(i)} \sum_l \tilde{G}_{lk} \frac{C_l^{(D)}}{C_l^{(i)}}. \quad (4.9)$$

We recast this formula slightly [\[6\]](#), to explicitly highlight the numerical deviation from the

target at each iteration as follows:

$$P_k^{(i+1)} = P_k^{(i)} \left[1 + \sum_l \tilde{G}_{lk} \frac{C_l^{(D)} - C_l^{(i)}}{C_l^{(i)}} \right]. \quad (4.10)$$

One can verify that by using normalized radiative kernel, \tilde{G}_{lk} , the overall normalization of both C_l and P_k is preserved.

4.3 Integral equation in action

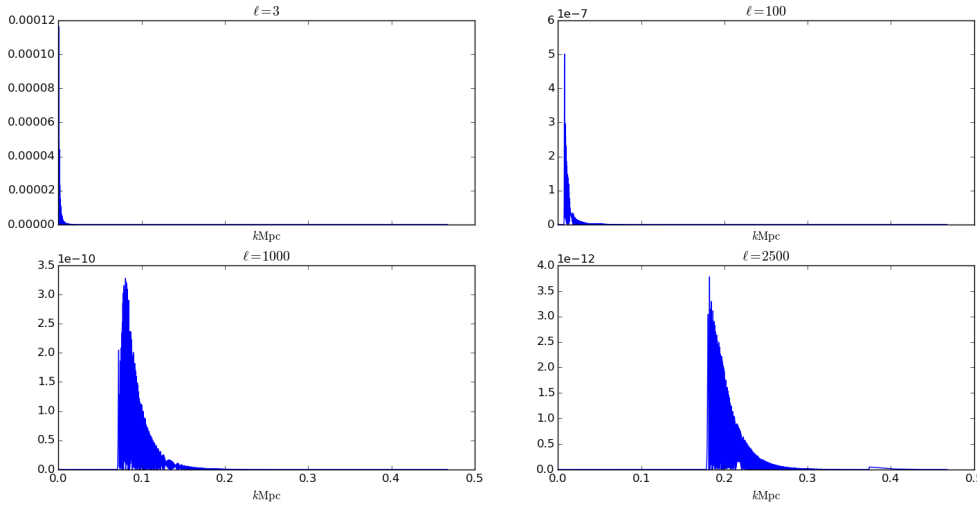


Figure 4.1: This figure represents the radiative transfer kernel for a few particular multipoles. Note how the function is non-zero only in a small region. This region is slightly displaced as the multipole changes however the function is zero-valued in a large section. Hence, the efficiency of the recovery of the PPS is different at different scales as we will see later.

At this point we are well equipped to go ahead and do some actual computations of angular power spectrum using CAMB. CAMB essentially calculates the integral defined in the previous section to compute the angular power spectrum. We make suitable modifications to the code to implement the improved Richardson Lucy deconvolution in CAMB itself. By default CAMB assumes the scale invariant power law model for the PPS. We use the temperature data from Planck 2015 release to do the iRLD and obtain a

free-form PPS that is subsequently convolved with the radiative transfer kernel to calculate C_l .

We then did a preliminary check to see if our RLD method could be applied successfully in its most basic form and scrutinize how the C_l corresponding to the recovered PPS compares with the C_l corresponding to the Power law PPS.

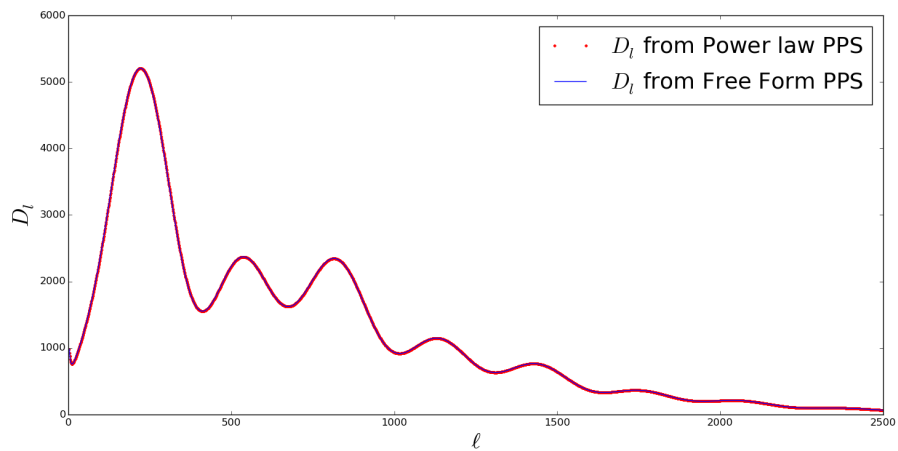


Figure 4.2: This figure represents a preliminary comparison between the two angular power spectra obtained from CAMB with different forms for PPS.

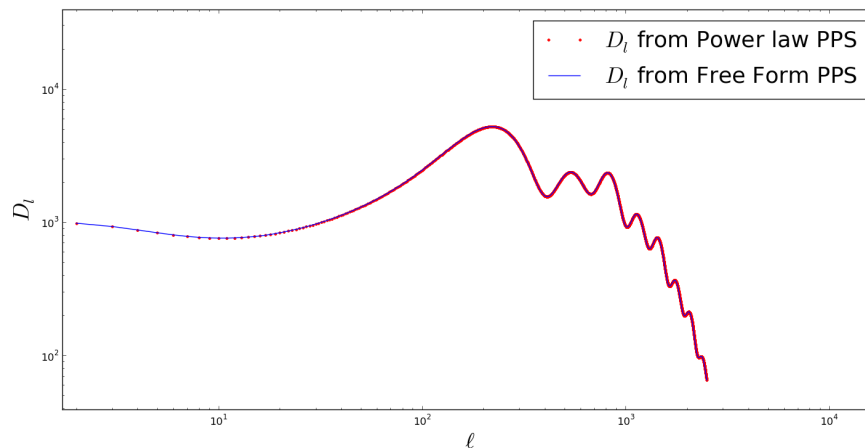


Figure 4.3: This figure represents the same curve above in a log-log scale to focus on the low l values.

4.4 Toy models

As a sanity check we ran the algorithm on known quantities. Consider a system of linear equations $Y = AX$, where X and Y are vectors and A is matrix. We begin with a sine curve that is represented by black in the plot below and try to recover it using RLD algorithm.

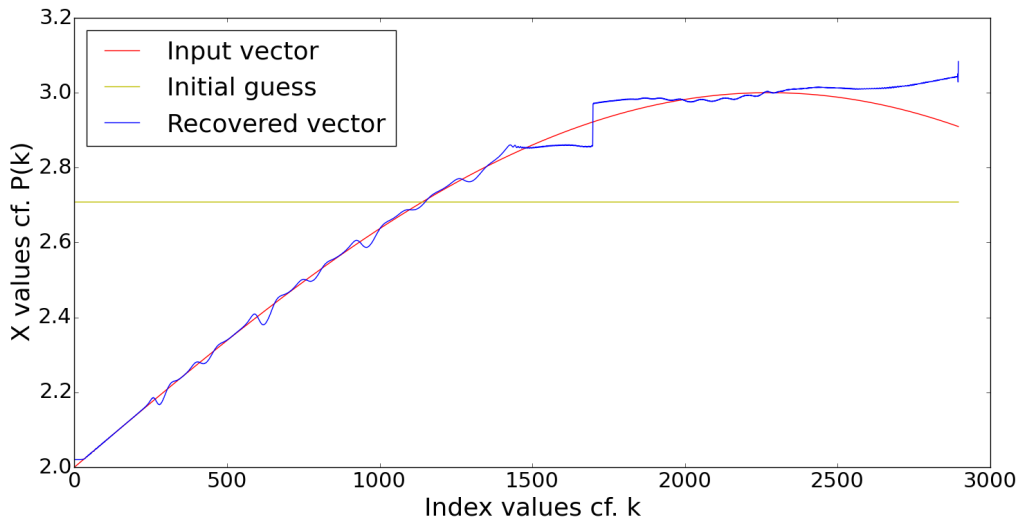


Figure 4.4: This figure represents the recovery of a peak of a sine wave using RLD algorithm in a toy model. The black line is the expected recovery, the blue line represents the curve recovered after about 100 iterations. The yellow line represents the initial guess.

4.5 Regularization term

We had earlier discussed about how our data is limited by Cosmic Variance at low multipole values l s and systematics at high multipole values l . We can not rely on the observations beyond these error bars. However, the standard Richardson Lucy Algorithm has no provisions for incorporating the information regarding errors. Hence we need to modify the existing algorithm appropriately to include a regularization term that ensures that this method does not start fitting features from the noise especially at large iterations.

As suggested by Souradeep et al. [6], the addition of a hyperbolic tangent (\tanh)

term can be used to diminish the contributions from those l values where there is high noise present. Consequently, the method will assign lesser weights to such l values, and thereby converge faster. This prescribed regularization term is by no means unique, but works adequately well and also results do not depend much on the specific form of the regularization term. Now our equation looks like,

$$P_k^{(i+1)} = P_k^{(i)} \left[1 + \sum_l \tilde{G}_{lk} \frac{C_l^{(D)} - C_l^{(i)}}{C_l^{(i)}} \tanh^2 \left[\frac{(C_l^{(D)} - C_l^{(i)})^2}{\sigma_l^2} \right] \right] \quad (4.11)$$

We demonstrate the impact of the inclusion of the regularisation terms below.

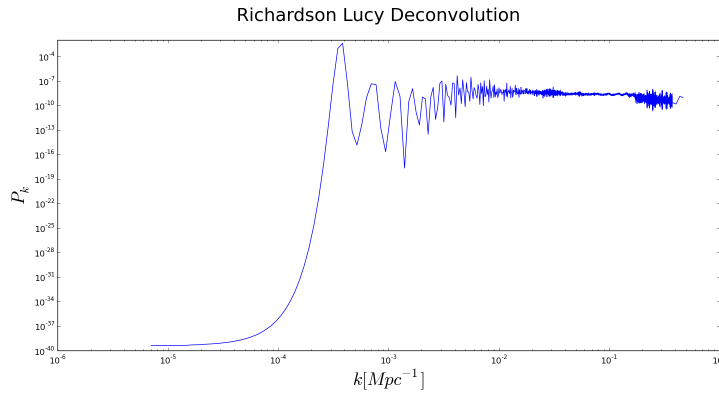


Figure 4.5: This figure demonstrates the PPS recovered after 100 iterations of the standard RLD. Due to the large fluctuations at small l values, the lower part of PPS keeps falling with iterations.

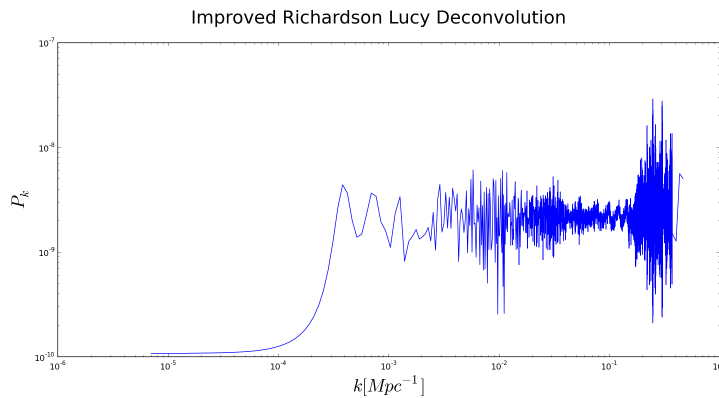


Figure 4.6: Here we have included the regularization term which is a tan hyperbolic function of a value that quantifies the error. This function has a range between 0 to 1.

4.6 Prior bias

Iterative methods are generally dependent on the initial conditions we choose. Therefore we need to be careful about our initial guess biasing our results. In our analysis, we use a uniform prior with no features so as to have a minimal bias on our results. In Bayesian analysis we obtain new posterior distribution based on availability of new data. The posterior distribution has input from both our prior assumption and the data in different weights. In our case we do not have much information present in our prior since it is a guess. We would therefore want it to have a minimal weight with data having more weight. This is exactly the case in RLD. We show that the method is prior independent. We use three different priors to demonstrate this.

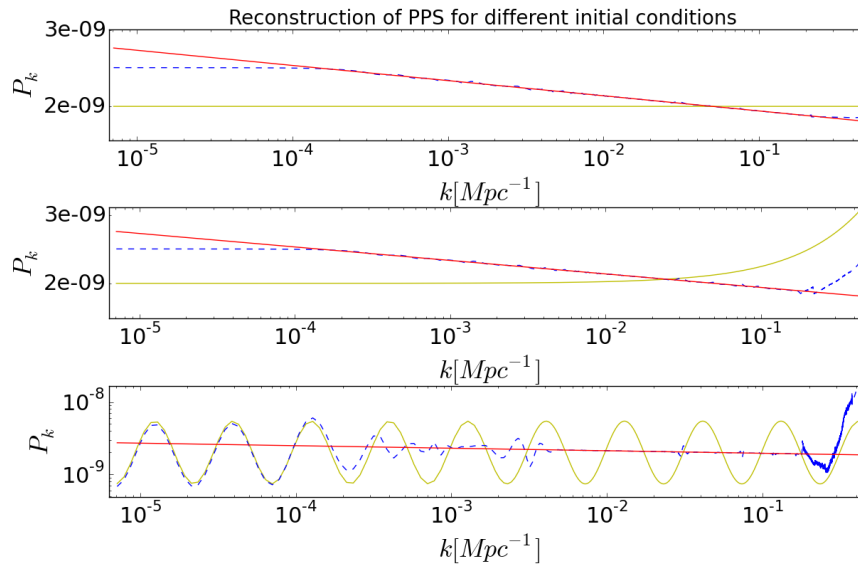


Figure 4.7: We demonstrate the prior independence by recovery of PPS using three different priors. The first uses a uniform prior, the second goes as e^k and the third goes as $\exp(\sin(\log(k)))$. Note that for the range between 5×10^{-4} and 10^{-1} and the PPS is recovered successfully in all the three cases.

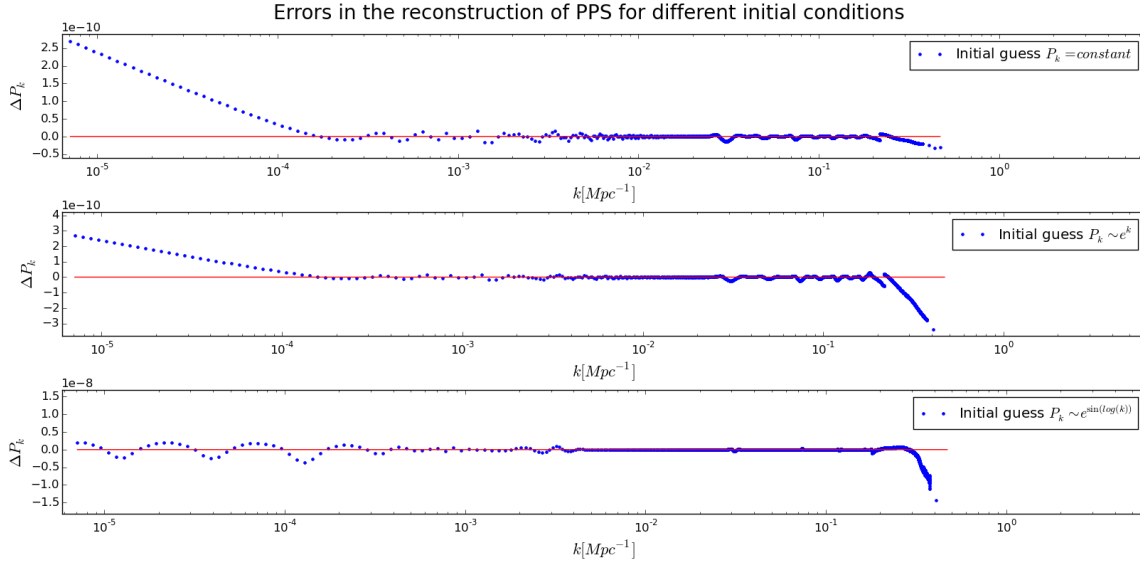


Figure 4.8: This figure shows the residuals from the plot above to highlight the efficiency of reconstruction at different l values.

4.7 Post processing

The iRLD method can leave some signatures on the recovered PPS due to residual fluctuations present in the data due to noise and discrete sampling. These features show up in the PPS as high frequency fluctuations that need to be smoothed out. There are several corrective measures that have been tested before like wavelet analysis, singular value decomposition and transforms using various filters. We implement a Gaussian filter with a suitable window to reduce the fluctuations. The filter is implemented by the following formula^[7],

$$P_k^{Smooth} = \frac{\sum_{k'=k_{min}}^{k_{max}} P_{k'}^{Raw} \times \exp \left[-\left(\frac{\log k' - \log k}{\Delta} \right)^2 \right]}{\sum_{k'=k_{min}}^{k_{max}} \exp \left[-\left(\frac{\log k' - \log k}{\Delta} \right)^2 \right]}. \quad (4.12)$$

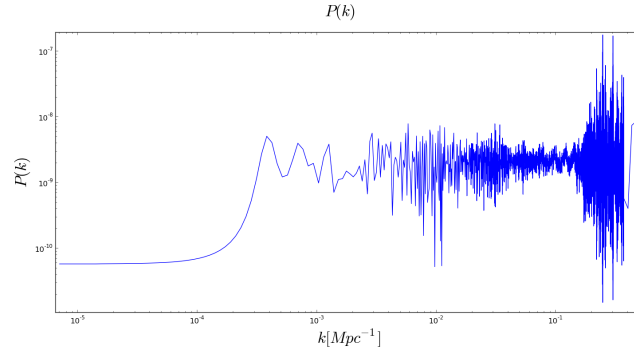


Figure 4.9: Without Gaussian smoothing

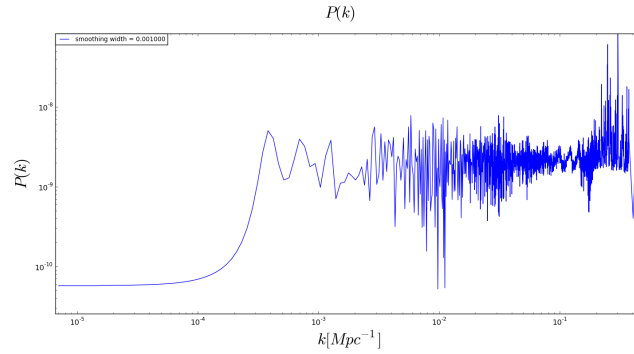


Figure 4.10: With Gaussian smoothing with a window size of 0.001 units

4.8 Convergence criteria

The RLD method being an iterative one we need to specify the criteria to stop the iterations. We would like to strike a balance between achieving sufficient accuracy and keeping the computation time minimal. As a convenient measure, we calculate the χ^2 value after each iteration. As expected, this value starts falling down, and when it almost saturates we terminate the iterations. Here, L represents the total multipole values we have, i.e., 2508.

$$\chi_i^2 = \frac{1}{L} \sum_l \frac{(C_l^D - C_l^i)^2}{\sigma_l^2} \quad (4.13)$$

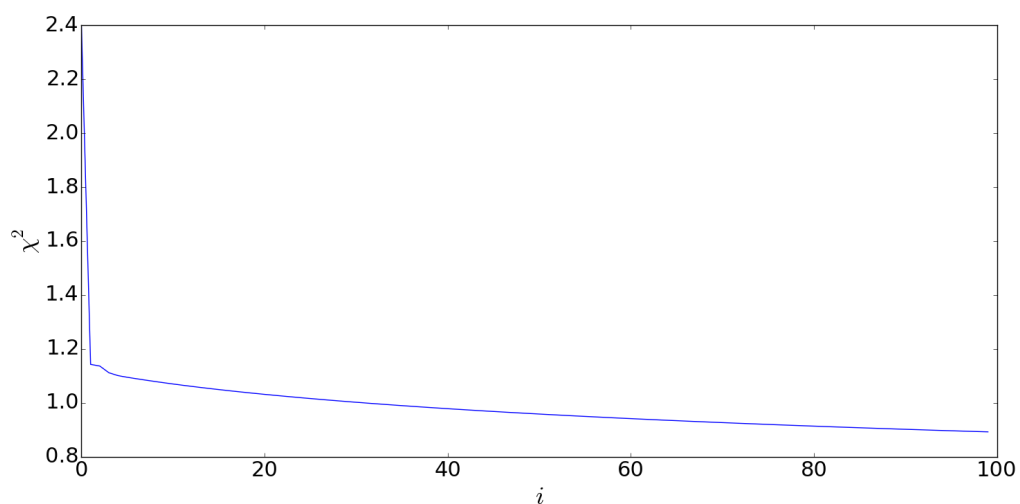


Figure 4.11: This figure depicts how χ^2 saturates after sufficient iterations.

4.9 Results

After having set the machinery for the iRLD algorithm, we test it on some simulated data. We first test the efficacy of this method by using it on a power spectrum that was injected by a power law PPS. The Power spectrum was generated by a code called CAMB[10].

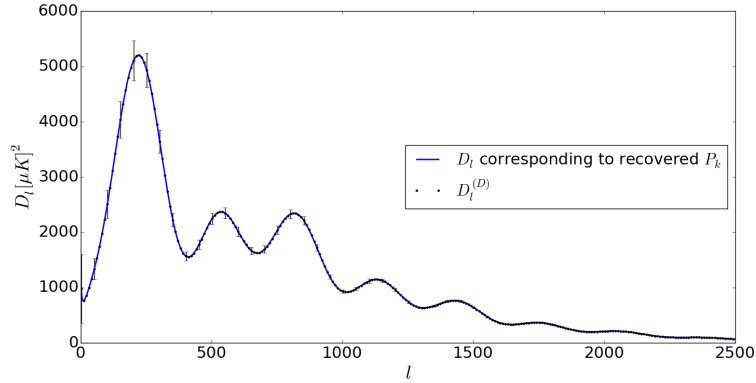


Figure 4.12: This figure compares the C_l corresponding to the recovered P_k (shown by the blue line) with the simulated C_l shown by the black dots. The error bars represent the cosmic variance at different l values. They are not shown for every l value to avoid cluttering.

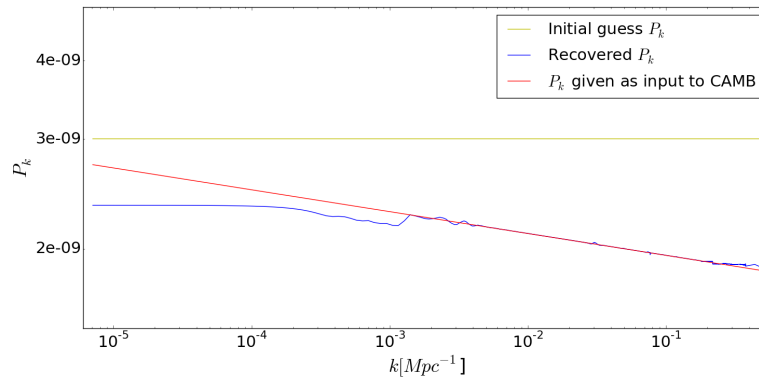


Figure 4.13: The recovered P_k is shown by the blue line. The yellow line represents the uniform prior, while the red line is the expected scale invariant power law P_k . Note that the reconstruction is not uniformly robust over the entire wavenumber range. This is consistent given the support of G_{lk} over the wavenumber.

It is apparent that iRLD method is not uniformly robust at all scales. We inject power law with two different features at three different k ranges and study the efficiency of this method.

We arrive at a conclusion that this method recovers the PPS fairly well in the range between 10^{-1} and 10^{-4} . This is due to lack of support of G_{lk} at the extreme ends and our recovery fails to capture features present in those regions.

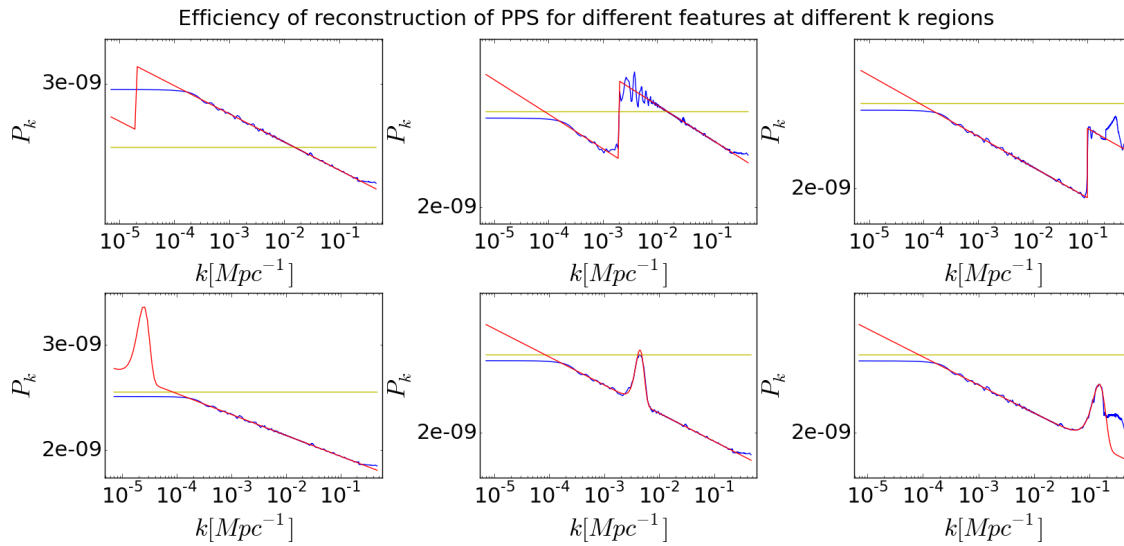


Figure 4.14: The efficiency of reconstruction is not uniform across the entire k range. We demonstrate this by introducing two kinds of features at three different k ranges as shown. Note that the method is insensitive to features at lower k values

Finally, we apply the RLD method on Planck binned and unbinned data from the Planck release of 2015. The advantage of using binned data is that since the l values are fairly wide apart, we have smoother looking curves and hence we will have lesser aberrations while the drawback being some amount of information loss. Note the reduction in the oscillations at larger l values in the case of unbinned data. The unbinned data, on the other hand, has lesser loss of information but it is very noisy. We use cubic spline interpolation to obtain data points for every l value in the case of binned angular power spectrum. We use both these datasets and look for common features.

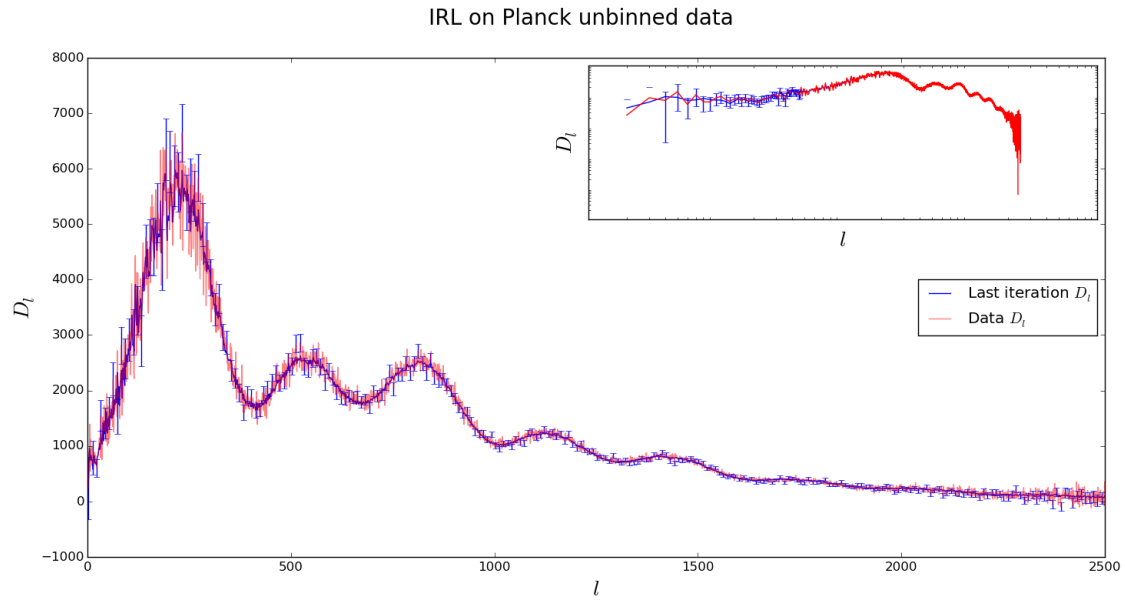


Figure 4.15: This figure shows the unbinned angular power spectrum from Planck 2015 data depicted in red and the reconstructed angular power spectrum depicted in blue. The in-plot shows the same curve in logarithmic scale to highlight the features in low l part.

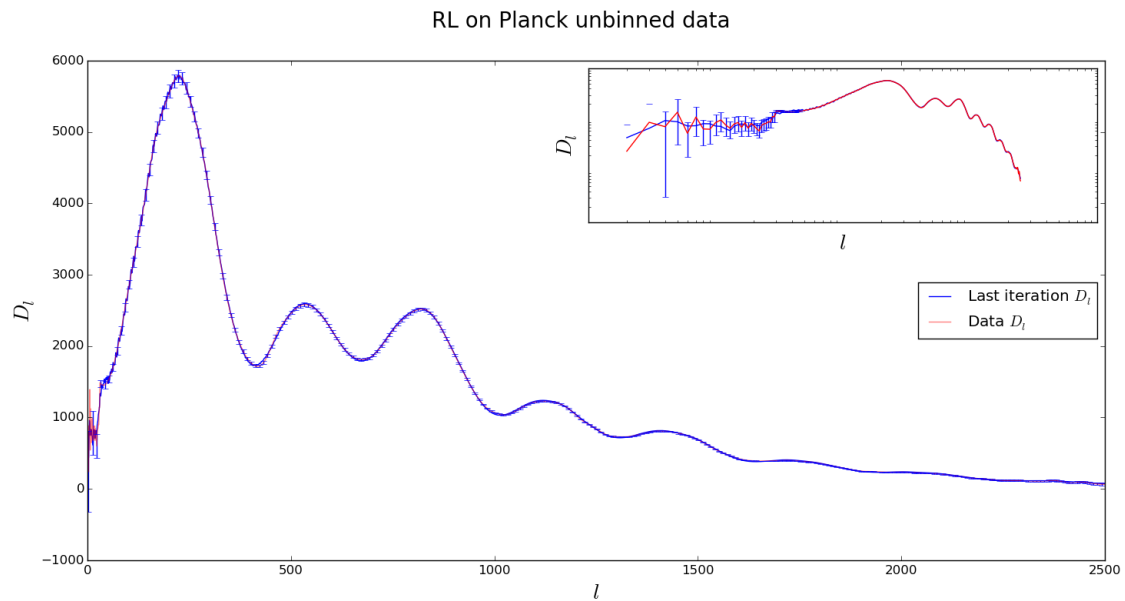


Figure 4.16: This figure shows the binned angular power spectrum from Planck 2015 data [\[1\]](#) depicted in red and the reconstructed angular power spectrum depicted in blue. The inplot shows the same curve in logarithmic scale to highlight the features in low l part.

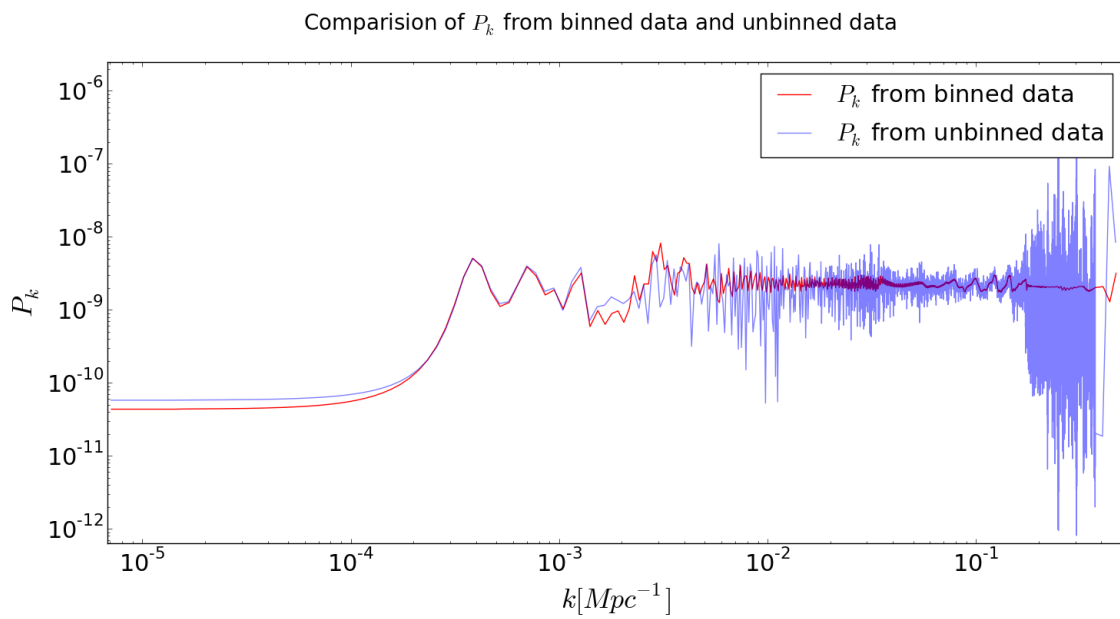


Figure 4.17: This figure compares PPS from binned and unbinned data Planck data. The unbinned data has data for larger number of multipole l sampled but also comes with high noise. On the other hand, we have lower noise in case of binned data but with limited l samples. However, the significant features like infrared cut-off and oscillations are apparent in both.

Chapter 5

Cosmological parameter estimation

In the last section we had assumed the best-fit values from the Planck 2015 [20] for the background cosmological parameters and then proceeded with the iRLD. However, it is well known that there is no preferred model for inflation and hence what model we use strongly biases our estimates of the background parameters inferred from CMB spectrum [16]. This calls for a more general approach, preferably a model independent technique to complement a parameter estimation. With the iRLD method, we aim to obtain revised estimates of the cosmological background parameters without the bias arising from the assumption of a model for the Primordial Power Spectrum(PPS). However, the computation of the radiative kernel for a given cosmology is a computationally expensive task. Therefore, we need to use smart, computationally efficient ways of sampling the parameter space such as using Markov Chain Monte-Carlo sampling methods.

5.1 Markov Chain Monte-Carlo techniques

Markov Chain Monte-Carlo methods are frequently used in Cosmology to obtain a fair sample of the posterior probability distribution in the multi-dimensional space of cosmological parameters. In situations where the exact analytical distribution is not known or it is computationally expensive to compute, we can estimate the distributions and its sta-

tistical properties by drawing a large number of random fair samples. Continuing in the Bayesian perspective as described in Chap. 3, we use the data obtained by observations to update our a prior knowledge about parameters to obtain a posterior state of beliefs by examining the likelihood of data given the parameters. Typically one runs multiple chains simultaneously. While constructing Markov chains is a straight forward process, care must be taken to set proper convergence criteria for all the chains. Typically one sets the convergence criteria while running several chains as the step at which the ratio of inter-chain to the intra-chain variance for all the parameters is less than unity. This criteria is also known as the Gelman-Rubin criteria[27]. There are several Monte-Carlo methods with different levels of sophistication and different range of applications, ex. Metropolis-Hastings algorithm, Gibbs sampling etc. In our analysis, the publicly available CosmoMC code makes use of the Metropolis-Hastings algorithm with modifications appropriate to our approach. [21].

5.2 Metropolis-Hasting algorithm

Metropolis-Hastings algorithm[26] is one of the simplest MCMC technique that is used to draw a sequence of random samples from a probability distribution $P(x)$ to estimate its statistics provided one can find another function $f(x)$ that is proportional to the density of P . At each iteration of the sampling, the next candidate is chosen based only on the current sampled point. The new candidate is accepted or rejected based on comparing the function $f(x)$ of the new and the currently accepted sample. If the current position is x and the new sample point under consideration is x' , then the acceptance ratio is

$$\alpha = \frac{f(x')}{f(x)} \quad (5.1)$$

Then we generate a random number n on $[0, 1]$. If $u \leq \alpha$, only then we accept the new candidate sample point. This method ensures that if the new candidate is more likely than the previous point than it is always accepted. Otherwise it is accepted with a probability that depends on how much drop in likelihood the newer point corresponds to. Thus we tend to stay in high density regions while not getting stuck in local minima.

5.3 Likelihood surfaces

We run the sampling algorithm on the 4-dimensional parameter space while doing an iRLD step at each point of the parameter space. We report significant deviations in the best-fit values for all the four parameters compared to those obtained by assuming the Power law model for the PPS. The preferred value of Baryon density and the acoustic scale parameter are higher than the previously reported values, while the other two parameters, the cold dark matter density and optical depth at reionization tend to prefer a value lower than expected as can be seen in the graphs below. The revised best fit values for $\Omega_b h^2$, $\Omega_c h^2$, τ and 100θ are 0.0259, 0.0733, 0.0345 and 1.0440 respectively. We obtain angular power spectrum that have significantly higher values of likelihood when we assume free-form PPS. In our analysis, we have used the hi_1_TT and low_1_TT (commander) likelihood data sets provided by Planck [23]. Since free-form PPS has higher degrees of freedom, we expect a larger area of parameter space to be acceptable and our results are consistent with this expectation.

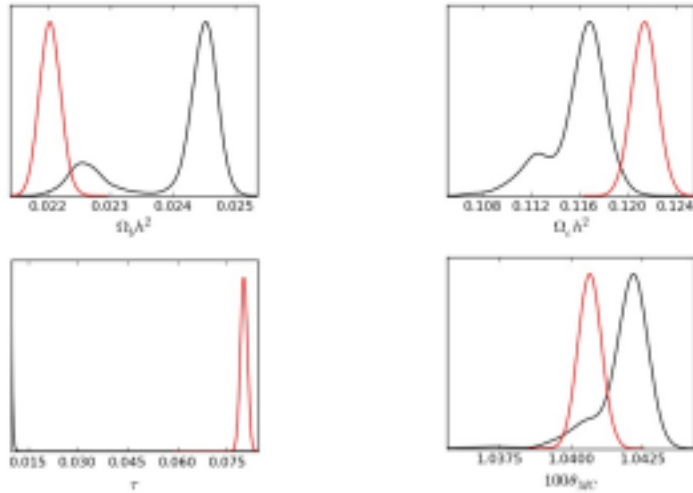


Figure 5.1: The figure represents the one dimensional marginalized likelihood of all the four background parameters obtained using free form of primordial spectrum (in red line) and using power law (in black line) using only the CMB temperature data from Planck 2015. The Y-axis shows the normalized marginalized 1-D probability of the cosmological parameter and runs from zero to unity at the peak of the distributions.

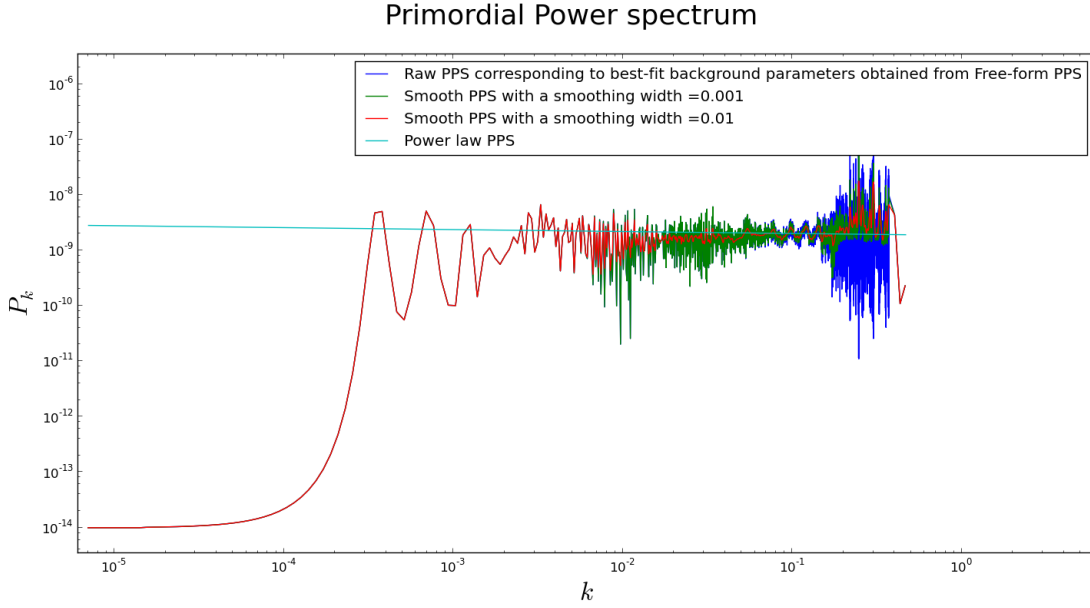


Figure 5.2: Reconstructed power spectrum corresponding to the revised best-fit values for the four background parameters are shown here. The recovered PPS has been smoothed with two different smoothing widths (red and green). The Power law PPS has also been plotted (in teal) for reference.

Parameter	Power law	Free form	Difference
$\Omega_b h^2$	0.02204 ± 0.00017	$0.0259^{+0.0028}_{-0.0023}$	0.00386
$\Omega_c h^2$	0.1214 ± 0.0011	0.0733 ± 0.0045	0.0481
$100\theta_{MC}$	1.04067 ± 0.00041	1.0440 ± 0.0017	0.00333
τ	0.0801 ± 0.0010	< 0.0345	> 0.0456

Table 5.1: Here we have tabulated the best-fit values for the background parameters along with $1\text{-}\sigma$ spread around it obtained using both the Power law model and the free-form PPS.

$\chi^2 = -2 \log \mathcal{L}$	Power law	Free form	Difference
Hi l TT	6062.38693227	5104.66223714	957.72469513
Low l TT	16.84863547	14.46326366	2.38537181
Total	6079.23556774	5119.1255008	960.11006694

Table 5.2: Here we have tabulated the effective χ^2 values for the angular power spectra obtained using both the Power law model and the free-form PPS. Note that the free form PPS has significant improvement in Likelihood compared to the Power law PPS.

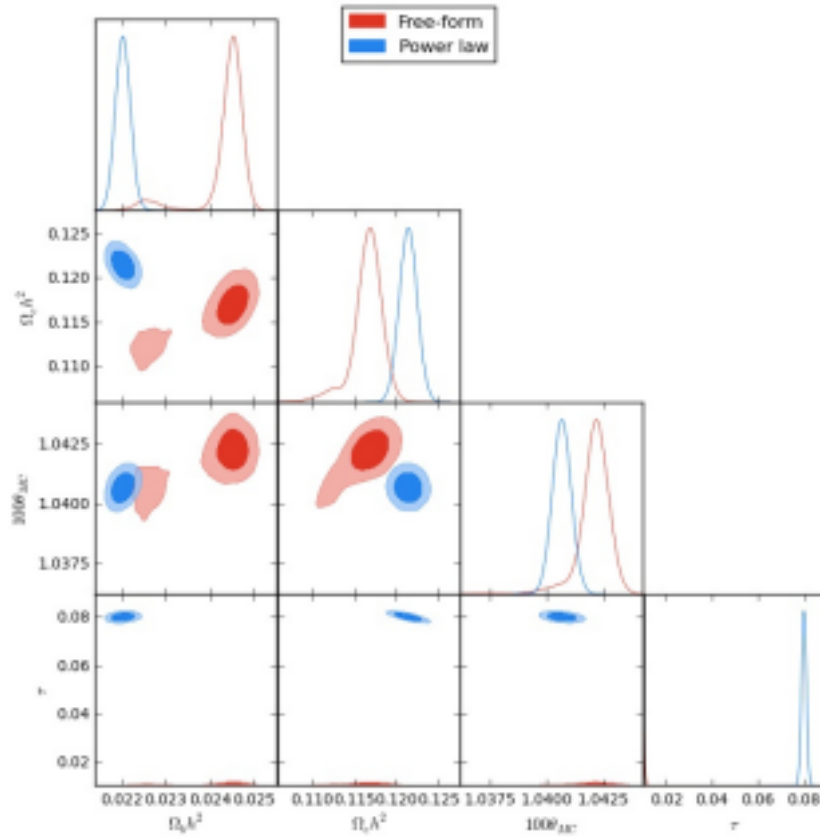


Figure 5.3: This figure compares the best-fit distributions for the background parameters. The results obtained using the Free-form PPS are represented by red and that obtained using Power law PPS are represented by blue. We obtain larger areas of accepted parameter space when we assume the free-form PPS as expected.

Chapter 6

Discussions and Conclusions

The period of last 50 years has witnessed a dawn of an era of precision cosmology. Increasingly sophisticated satellites like WMAP, Planck have provided us a rich set of CMB data to work with. This provides us with an invaluable means to test theories about early universe and particularly reach a consensus on what inflationary mechanism was under operation. The Primordial Power Spectrum(PPS) is not directly observable, however, the angular power spectrum of CMB is a convolution of PPS with a radiative transfer kernel. This is an observable that is measured with great accuracy on a wide range of scales. Therefore we are motivated to reconstruct the PPS directly from the data without any bias from the theoretical model.

In the first part of the project, we apply a model-independent method, namely the improved Richardson-Lucy Deconvolution algorithm to reconstruct the Primordial Power Spectrum using the Planck 2015 temperature data with cosmological parameters fixed to the best fit values obtained assuming the Power law PPS. We have assumed a spatially flat universe with Λ CDM model of Cosmology. We observe that the iRLD method is independent of the initial guess for PPS. We also note that the recovery is efficient at scales between 10^{-1} and 10^{-4} . This was explained by observing that the support of the radiative kernel, G_{lk} was restricted to this regime. We smoothen the rapid fluctuations since they are due to the noise present in the data and are not physically significant by running a Gaussian smoothing filter. We compare the reconstructions from Planck binned and

unbinned data and look for matching features. The recovered spectrum has several significant deviations from the previously assumed power law model for PPS, particularly the infrared cut-off and some oscillatory features consistent with results obtained earlier [19, 17]. This motivates us to revise our best-fit estimates of the cosmological background parameters with the free form power spectrum.

In the second half of this project we relax the assumptions of the best fit values for the background parameters and instead explore a 4-dimensional parameter space, doing a iRLD at each randomly chosen point. Since this is a computationally taxing job, we employ techniques of Markov Chain Monte Carlo to sample the parameter space. We develop our own MCMC code. However, we use a publicly available code called CosmoMC that uses the Metropolis Hastings algorithm to do the sampling since it is more efficient. We obtain new landscapes of the posterior distributions for the background cosmological parameters given the Planck temperature data and parameters.

The features we obtained in the reconstructed PPS can be used in inflationary model building such as the punctuated inflation etc., to look for new theories whose predictions match with the data more accurately. We also showed that the previously assumed form of the PPS biases the constraints obtained on the cosmological background parameters. With the power law model, it was not possible to achieve suitably low value of χ^2 in certain regions of the parameter space. But with the free-form PPS, we achieve a significant improvement in the χ^2 . It opens up a larger space of viable cosmological parameters and hence motivates us to revisit our theories of early universe scenarios.

We conclude by suggesting some future prospects of this work. In our analysis, we have only used the temperature data. We could, in principle, include the polarization data sets (TE, EE, BB etc) as well to improve our reconstruction of PPS. This involves including theoretically computable radiative kernels for these additional angular power spectra. The PPS should stay the same theoretically. Working with a larger data set will certainly improve the signal to noise ratio and improve our parameter estimates. However, we defer the inclusion of polarization data till the Planck collaboration publicly releases the final CMB polarization data. We have ignored the effects of lensing on CMB. We could achieve more reliable estimates by taking the lensing spectra into consideration. Another potential improvement that could be done is to reduce the computational time required

to do the sampling. The iRLD method used data from all the multipoles to do the deconvolution. It takes about four days to do a 4-dimensional parameter sampling with iRLD at each point. We could apply techniques of Single Value Decomposition (SVD) to reduce the number of calculations required without losing much information and thereby reduce the computational time.

Bibliography

- [1] Francois R. Bouchet, on behalf of the Planck collaboration for the results. The Planck mission. arXiv:1405.0439 [astro-ph.CO]
- [2] Wilkinson Microwave Anisotropy Probe. <https://lambda.gsfc.nasa.gov/product/wmap/current/wmap/current/index.cfm>.
- [3] L. B. Lucy. An iterative technique for the rectification of observed distributions. The Astronomical Journal, Vol 79, No. 6 (1974).
- [4] Tarun Souradeep. CMB notes on theory of PPS and transfer functions.
- [5] U.Seljak and M. Zaldarriaga. A line of sight integration approach to CMB anisotropies. Astrophys J., 469, 437 (1996).
- [6] Arman Shafieloo and Tarun Souradeep. Primordial power spectrum from WMAP. PhysRev D70 (2004).
- [7] Dhiraj Kumar Hazra, Arman Shafieloo, Tarun Souradeep. Primordial power spectrum from Planck. JCAP 11 (2014).
- [8] Paul Hunt and Subir Sarkar. Reconstruction of the primordial power spectrum of curvature perturbations using multiple data sets. Journal of Cosmology and Astroparticle Physics, Volume 2014, January 2014.
- [9] C. P. Ma and E. Bertschinger. Cosmological Perturbation Theory in the Synchronous and Conformal Newtonian Gauges. Astrophysical Journal v.455, p.7 (1995).
- [10] Antony Lewis and Anthony Challinor. <http://camb.info/>.

- [11] Quantum Theory of Angular Momentum. By D A Varshalovich, A N Moskalev, V K Khersonskii. World Scientific Publishing.
- [12] Modern cosmology. By Scott Dodelson. Academic Press.
- [13] Rita Sinha and Tarun Souradeep. Post-WMAP assessment of infrared cutoff in the primordial spectrum from inflation. Physical Review D 74, 043518 (2006).
- [14] A.A. Starobinsky. Beyond The Simplest Inflationary Cosmological Models. J. Exp. Theo. Phys. Lett. 55 (1992) 489.
- [15] Tarun Souradeep. Cosmology with cosmic microwave background anisotropy. Pragma journal of physics, Vol. 67, No. 4.
- [16] Dhiraj Kumar Hazra, Arman Shafieloo, Tarun Souradeep. Cosmological parameter estimation with free-form primordial power spectrum. Phys. Rev. D 87, 123528.
- [17] Primordial power spectrum: a complete analysis with the WMAP nine-year data. Dhiraj Kumar Hazra, Arman Shafieloo, Tarun Souradeep. Journal of Cosmology and Astroparticle Physics, Volume 2013, July 2013.
- [18] Features in the primordial power spectrum? A frequentist analysis. Jan Hamann, Arman Shafieloo, Tarun Souradeep. Journal of Cosmology and Astroparticle Physics, Volume 2010, April 2010.
- [19] Estimation of Primordial Spectrum with post-WMAP 3 year data. Arman Shafieloo, Tarun Souradeep. Phys. Rev. D 78, 023511.
- [20] Planck collaboration. Planck 2015 results XI. CMB power spectra, likelihoods, and robustness of parameters. Astronomy and Astrophysics, Volume 594, October 2016.
- [21] CosmoMC. www.cosmologist.info/cosmomc/readme.html.
- [22] 2015 CMB spectra and likelihood code. www.wiki.cosmos.esa.int/planckpla2015.
- [23] Planck Legacy Archive <https://pla.esac.esa.int>
- [24] A Measurement of Excess Antenna Temperature at 4080 Mc/s. Penzias, A. A.; Wilson, R. W. Astrophysical Journal, vol. 142, p.419-421.

- [25] Maximum Entropy deconvolution of Primordial Power Spectrum. Gaurav Goswami, Jayanti Prasad. *Phys. Rev. D* 88, 023522 (2013).
- [26] Hastings, W.K. (1970). "Monte Carlo Sampling Methods Using Markov Chains and Their Applications". *Biometrika*. 57 (1): 97-109.
- [27] Andrew Gelman and Donald B. Rubin. Inference from Iterative Simulation Using Multiple Sequences. *Statist. Sci.* Volume 7, Number 4 (1992), 457-472.